UC Davis
UC Davis Previously Published Works

Title

Engineering functional anisotropy in fibrocartilage neotissues

Permalink

Journal

ISSN

Authors

MacBarb, Regina F
Chen, Alison L
Hu, Jerry C
et al.

Publication Date

DOI

Contents lists available at ScienceDirect

Biomaterials

journal homepage: www.elsevier.com/locate/biomaterials

Engineering functional anisotropy in fibrocartilage neotissues

Regina F. MacBarb [a], Alison L. Chen [a], Jerry C. Hu [a], Kyriacos A. Athanasiou [a, b, *]

[a] Department of Biomedical Engineering, University of California Davis, One Shields Avenue, Davis, CA 95616, USA
[b] Department of Orthopedic Surgery, University of California Davis, 4860 Y Street, Suite 3800, Sacramento, CA 95817, USA

ARTICLE INFO

ABSTRACT

The knee meniscus, intervertebral disc, and temporomandibular joint (TMJ) disc all possess complex geometric shapes and anisotropic matrix organization. While these characteristics are imperative for proper tissue function, they are seldom recapitulated following injury or disease. Thus, this study's objective was to engineer fibrocartilages that capture both gross and molecular structural features of native tissues. Self-assembled TMJ discs were selected as the model system, as the disc exhibits a unique biconcave shape and functional anisotropy. To drive anisotropy, 50:50 co-cultures of meniscus cells and articular chondrocytes were grown in biconcave, TMJ-shaped molds and treated with two exogenous stimuli: biomechanical (BM) stimulation via passive axial compression and bioactive agent (BA) stimulation via chondroitinase-ABC and transforming growth factor-β1. BM + BA synergistically increased Col/WW, Young's modulus, and ultimate tensile strength 5.8-fold, 14.7-fold, and 13.8-fold that of controls, respectively; it also promoted collagen fibril alignment akin to native tissue. Finite element analysis found BM stimulation to create direction-dependent strains within the neotissue, suggesting shape plays an essential role toward driving *in vitro* anisotropic neotissue development. Methods used in this study offer insight on the ability to achieve physiologic anisotropy in biomaterials through the strategic application of spatial, biomechanical, and biochemical cues.

© 2013 Elsevier Ltd. All rights reserved.

1. Introduction

Tissue engineering offers much promise toward developing clinically relevant repair and/or replacement tissues for those damaged by injury or disease. Specifically relating to cartilage, much progress has been made within the last decade toward achieving such a goal [1]; engineering efforts have led to the development of biomechanically robust articular cartilage capable of both *in vivo* integration and maturation [2–8]. Progress in engineering fibrocartilage, such as the knee meniscus, intervertebral disc, and temporomandibular joint (TMJ) disc, however, has been hindered by their comparatively complex geometric shape and anisotropic matrix organization, both of which have proven especially difficult to fully recapitulate *in vitro*. Considering the inability of fibrocartilages to self-repair following injury and disease as well as the current lack of clinically available treatment options, efforts to generate neo-fibrocartilage capturing both the external and internal structural features of the target tissue are imperative to engineering implants with clinical feasibility.

Recent efforts toward generating the anatomical shape of fibrocartilaginous tissues most commonly utilize a scaffolding material formed into the native tissue's geometric shape [9–15]. With regards to matrix anisotropy, electrospinning has been used to align either organic or inorganic fibers as a template for directed tissue growth [16–18]. While such scaffold-based methods have shown potential toward generating anatomically shaped implants, fully capturing the true ECM organization within these shape-specific neotissues remains elusive. Furthermore, scaffolds have been associated with certain drawbacks that can detract from both proper geometry and anisotropy. For instance, mismatched scaffold biodegradability and tissue formation can lead to irregularly shaped tissues, while stress-shielding can lead to incorrect ECM alignment. Other issues, including biocompatibility and hindrance of cell-to-cell communication, are also of concern. As an alternative to scaffold-use, a scaffold-free, self-assembling approach to fibrocartilage tissue engineering has been developed: seeding co-cultures of articular chondrocytes (AC) and meniscus cells (MC) at high densities in non-adherent molds results in the formation of robust neotissue [19,20]. Use of these non-adherent molds with different cell densities and ratios provides the ability to generate

constructs of different functional properties, shapes, sizes, and thicknesses [21—23]. Thus, the self-assembling process presents as a promising system to drive *in vitro* tissue formation in a specific, organized manner.

In vitro development of scaffold-free neofibrocartilage promotes both cell−cell and cell−matrix interactions and signaling, providing a bioactive system that greatly enhances cellular sensitivity to the surrounding microenvironment [24]. In addition to recapitulating native tissue morphogenesis [25], the self-assembling process also enables cells to respond to *in vitro* biomechanical and biophysical stimulation during tissue development in a more physiologic manner. Natively, cells sense and respond to such stimuli by adapting their extracellular matrix (ECM), and thus function, to accommodate external stressors [26−28]. It, therefore, follows that if the correct cues are applied to shape-specific, self-assembled fibrocartilage early during *in vitro* development, the tissue will be driven toward developing an ECM mimicking the architectural organization, size, and shape of native tissues.

Previous work has identified several important factors to enhance the functionality of self-assembled fibrocartilage. Transforming growth factor-β1 (TGF-β1) is an anabolic, biochemical stimulus that has been shown to increase overall glycosaminoglycan (GAG) and collagen content of engineered neocartilage, increasing neotissue functional properties [22]. The biophysical effect of the catabolic agent chondroitinase-ABC (C-ABC), on the other hand, is dependent on its ability to deplete GAG, inducing maturational growth of constructs and ultimately promoting the formation of a more functional collagen network capable of bearing greater tensile properties [29]. Combining these agents has been shown to recreate a more physiologic GAG:collagen ratio, resulting in synergistically enhanced tensile properties in engineered fibrocartilage [6,20]. Other work has highlighted the importance of biomechanical stimuli for enhancing neotissue development, finding self-assembled neotissue to be most responsive to such stimulation during the first 2 wk of neotissue development, specifically from $t = 10-14$ d [30,31]. Earlier than this time point, the self-assembled matrix has been shown to be not as well formed [25], leaving the cells vulnerable to the mechanical load; later than this time point, the construct's metabolic activity has been shown

to begin to decline [25], rending the construct less capable of responding to the load. Capitalizing on this critical window, therefore, recent work has found passive axial compressive loading during $t = 10-14$ d of culture to significantly enhance the functional properties of flat neocartilage constructs [32]. While these agents all present with much promise toward enhancing the development of flat neofibrocartilage constructs, their ability to promote ECM organization and enhance overall functional properties of shape-specific fibrocartilages remains unknown.

Of the various fibrocartilages found in the body, the TMJ disc presents with a unique biconcave shape possessing distinct regions of anisotropic collagen alignment. Collagen, which makes up an estimated 83% of the dry weight and 37% of the wet weight of the TMJ disc [33], aligns anteroposteriorly in the middle zone of the disc and circumferentially around the disc's periphery (Fig. 1A) [34]. This internal organization of collagen is imperative to the TMJ disc's ability to distribute peak forces imparted by the articulating surfaces of the jaw joint. The disc's biconcave geometry is likewise important, as it allows the highly incongruent articulating surfaces of the TMJ to mesh in a physiologically and mechanically efficient manner. Past work has viewed the TMJ disc as a trampoline-type structure [35,36], separating the disc into two distinct zones: 1) a middle zone, and 2) the surrounding band region. Viewing the disc in this manner is representative of the physiologic stress fields the disc faces within the TMJ and directly correlates with preferential collagen alignment in the respective zones. Thus, similar to a trampoline, the thicker band region of the TMJ disc acts as a supportive, compressive load-bearing system, while the thinner center region mainly distributes tensile loads. With such a strong correlation between structure and function, it is crucial that efforts are developed to not only match the bulk functional properties of engineered tissues such as the TMJ disc, but to also capture the tissue's internal ECM architecture and external anatomical form.

The overall objective of this study was to employ a combination of external stimuli to drive the development of fibrocartilaginous ECM capturing both the gross and molecular structural features of native tissues. For this purpose, self-assembled TMJ discs were chosen as a model system, as this biconcave tissue exhibits distinct regions of anisotropic collagen alignment that directly translate to
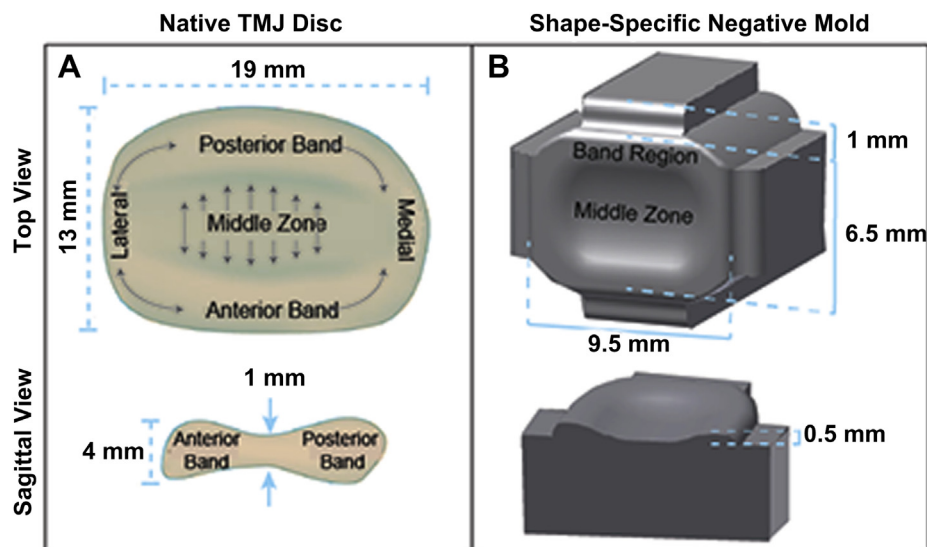

Fig. 1. Schematic of native TMJ disc (A) showing its biconcave shape and collagen fibril alignment to be anteroposterior in the middle zone of the disc, and circumferential around the band region, as represented by gray arrows. Schematic of TMJ shape-specific negative mold (B), having an aspect ratio of 1.5 in the mediolateral-anteroposterior direction from a top view and an average ratio of 2.5 between the band region and middle zone from a sagittal view, to create molds representing a geometric scaled-down version of the native TMJ disc. Note: figure not drawn to scale.

its anisotropic biomechanical functionality. Previous work has found the TMJ disc to be an improbable cell source due to its low cellularity and the poor matrix production of the isolated cells *in vitro* [33,37]; recent efforts to engineer TMJ disc fibrocartilage have therefore utilized co-cultures of MC and AC [20,22]. With both biomechanical and biochemical cues known to be influential factors toward *in vivo* fibrocartilage morphogenesis, this study examined the interaction of two exogenous stimuli on 50:50 MC:AC co-cultures grown in TMJ disc shape-specific wells: 1) biomechanical (BM) stimulation in the form of passive axial compression, and 2) bioactive agent (BA) stimulation via a regimen of the biophysical agent C-ABC and the biochemical agent TGF-β1. Overall, it was hypothesized that treating shape-specific constructs with both BM and BA cues would drive *in vitro* fibrocartilage morphogenesis toward tissue-specific geometric shape and anisotropic functional properties.

2. Materials and methods

2.1. TMJ shape-specific molds

The geometric aspect ratios of the native TMJ disc were used to design negative mold well makers. Specifically, an aspect ratio of 1.5 in the mediolateral:anteroposterior (ML:AP) dimensions from a top view and an average band:middle zone (B:MZ) ratio of 2.5 from a sagittal view was used (Fig. 1B). Negative molds were printed using an Objet260 Connex™ Compact Multi-Material 3D Printer (Objet Ltd., Minneapolis, MN and Rehovot, Israel) with a rigid Objet VeroBlack™ material. To make the shape-specific agarose wells, the 3D-printed negative molds were placed into 1.6 ml of molten 2% agarose in a 24-well plate (Fig. 2A). Once the agarose gelled, the negative molds were removed. The resulting shape-specific wells were then moved into 6 well plates and submerged in culture medium consisting of DMEM, 1% PSF, 1% non-essential amino acids, 100 nM dexamethasone (Sigma, St. Louis, MO), 1% ITS+ (BD Scientific, Franklin Lakes, NJ), 40 μg/ml L-proline, 50 μg/ml ascorbate-2-phosphate, and 100 μg/ml sodium pyruvate (Fischer Scientific, Pittsburgh, PA) for 2 d to ensure that the agarose was fully saturated with medium prior to seeding. To form the 3D shape of the TMJ disc-shaped constructs, agarose top pieces specifically formed to sit on top of the constructs within the agarose wells were also created using 3D-printed negative molds, forming TMJ shape-specific agarose well assemblies.

2.2. Chondrocyte isolation and self-assembly of TMJ shape-specific constructs

Immature AC from the distal femoral condyles and trochlear grove and MC from the knee menisci were harvested from calves and stored in liquid nitrogen until seeding, as previously described [20]. To form constructs, AC and MC were quickly defrosted, combined in a 1:1 mixture, and self-assembled within the TMJ shape-specific agarose wells at 12 M cells/well at $t = 0$ h. The cells coalesced into constructs by $t = 4$ h, and at $t = 3$ d, the agarose top pieces were capped over the constructs within each well (Fig. 2B–D). Constructs remained fully confined in the TMJ shape-specific agarose assembly within 6 well culture plates for the entire 5 wk culture period. During this time, constructs were fed 6 ml of culture medium every other day.
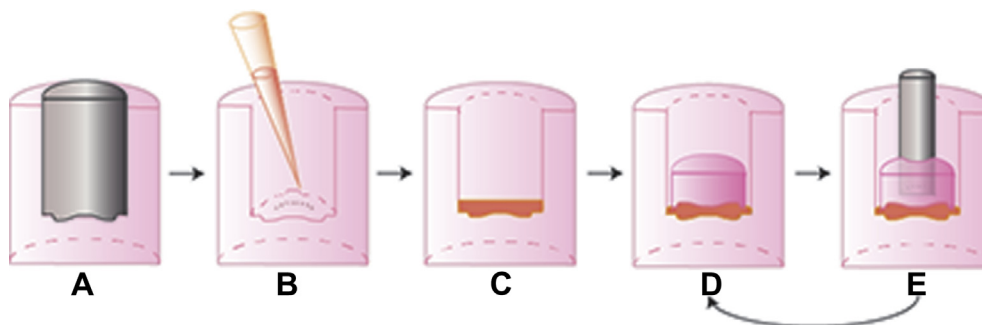
2.3. Exogenous stimulus

This study employed both BM (passive axial compression) and BA (C-ABC + TGF-β1) stimulation. For the BM stimulus, a 5-mm diameter, 1-cm long, 1-g, porous, sintered steel post corresponding to a 0.5 kPa stress was placed on top of the constructs in the agarose top piece from $t = 10$–14 d (Fig. 2E) [32]. BA stimulated constructs received 2 U/ml C-ABC (Sigma–Aldrich, St. Louis, MO) in culture medium for 4 h at $t = 21$ d in addition to TGF-β1 (PeproTech, Rocky Hill, NJ) administered continuously at 10 ng/ml for the entire culture duration [20]. Since C-ABC functions by temporarily depleting the GAG content from the neotissue, allowing for reorganization of a more functional collagen matrix, it should be applied after sufficient ECM accumulation has occurred. Based on prior studies [25], this corresponds with the time it takes the construct to fully fill the well. Therefore, the engineered TMJ discs were treated with C-ABC when constructs fully filled the well ($t = 21$ d). To investigate the interaction of the exogenous stimuli on TMJ shape-specific constructs, a two-factor (construct region and exogenous stimulus), full-factorial study design with $n = 6$ per group was employed. The construct region factor comprised the following levels: band region and middle zone. The exogenous stimulus factor consisted of the following levels: control, BM, BA, and BM + BA. At $t = 5$ wk, constructs were removed from culture and assayed as described below.

2.4. Native TMJ disc harvest

To serve as an internal control and to provide a direct comparison for where the engineered neotissue stands in relation to native discal tissue, TMJ discs were isolated from four, 4–6 month old juvenile pigs (Yosemite Meat Co., Modesto, CA). Upon removal, discs were wrapped in gauze soaked with protease inhibitor and stored at −20 °C until testing.

2.5. Histology and immunohistochemistry (IHC)

Samples were frozen in HistoPrep (Fisher Chemical, Vernon Hills, IL) and sectioned at 12 μm. Slides were fixed in formalin and stained with Safranin-O/Fast Green for GAG or Picrosirius Red for collagen. Picrosirius Red-stained slides were also viewed under polarized light to visualize collagen fibril orientation and alignment. For IHC, slides were fixed in 4 °C acetone and stained for collagen I or collagen II as previously described [20].

2.6. Biochemistry

Samples were blotted dry and wet weights were taken; following lyophilization for 48 h, dry weights were taken. Samples were digested using pepsin-elastase [38] at 65 °C overnight. Digests were assayed using a cholramine-T hydroxyproline assay with a SIRCOL collagen assay standard (Accurate Chemicals, Westbury, NY) for total collagen, and with a dimethylmethylene blue dye-binding assay kit (Biocolor, Newtownabbey, Northern Ireland) for GAG content.

2.7. Stress-relaxation compressive testing

An Instron uniaxial testing machine (Model 5565, Canton, MA) was used to collect unconfined, stress-relaxation data from 2 mm biopsy punches taken from the peripheral bands and the middle zones of both the TMJ disc-shaped constructs and native tissue. Data were fit to a Kelvin solid model using Matlab (Mathworks, Natick, MA) to calculate the viscoelastic properties, including both the relaxation modulus (E_r) and the instantaneous modulus (E_i), as previously described [20].

Fig. 2. 3D-printed negative molds were placed into 1.6 ml of molten 2% agarose in a 24-well plate to form shape-specific wells (A), which were then seeded with a 1:1 ratio of meniscus cells to articular chondrocytes (B), and allowed to settle and fill in the well (C). At $t = 3$ d, agarose top pieces were placed on top of the constructs to induce the biconcave shape, forming TMJ shape-specific agarose well assemblies (D), which the constructs remained in for the entire culture duration. For constructs receiving the biomechanical stimulus, a 1 g sintered steel post was molded into the agarose top piece and placed on constructs (E) from $t = 10$–14 d, after which the post was removed and replaced with an agarose top piece (D) for the remainder of culture.

Table 1
Neotissue properties at $t = 5$ wk. Values marked with different letters within each category are significantly different ($p < 0.05$), with A > B > C. ML = mediolateral, AP = anteroposterior, B = band, MZ = middle zone.

Parameter	Control	BM	BA	BM + BA
ML major diameter (mm)	9.4 ± 0.4^A	9.1 ± 0.4^A	7.5 ± 0.3^B	7.5 ± 0.2^B
AP major diameter (mm)	5.7 ± 0.4^A	5.4 ± 0.3^{AB}	5.0 ± 0.3^{BC}	4.9 ± 0.2^C
ML minor diameter (mm)	6.8 ± 0.4^A	6.9 ± 0.3^A	5.4 ± 0.2^B	5.6 ± 0.2^B
AP minor diameter (mm)	3.2 ± 0.3^A	2.9 ± 0.2^{AB}	2.7 ± 0.3^B	2.6 ± 0.3^B
B thickness (mm)	1.1 ± 0.1^A	1.1 ± 0.3^A	0.6 ± 0.1^B	0.7 ± 0.1^B
MZ thickness (mm)	0.5 ± 0.1^A	0.4 ± 0.1^A	0.2 ± 0.1^B	0.3 ± 0.1^B
Whole construct wet weight (mg)	68.2 ± 3.7^A	63.3 ± 3.0^B	26.4 ± 2.2^C	27.6 ± 2.0^C

2.8. Uniaxial tensile testing

Tensile testing using a uniaxial testing machine (Test Resources, Shakopee, MN) was conducted on dog bone-shaped samples. Both engineered and native discs were tested mediolaterally in their posterior band and anteroposteriorly in their intermediate zone. For engineered tissue, both ends of the dog-boned-sample were glued to a paper frame, which was then clamped into machines grips; for native tissue, the ends of the dog-boned-sample were directly clamped. The gauge length was measured as the distance between the glued ends of the paper frame for engineered tissue and as the distance between the machine grips holding the native tissue. The machine then applied a 1% per second strain rate of the gauge length until failure. The Young's modulus (E_Y) was calculated from the linear portion of the resulting stress vs. strain data, while the ultimate tensile strength (UTS) was recorded as the peak of the linear region of this curve.

2.9. Scanning electron microscopy (SEM)

Neotissue was dehydrated in ascending ethanol and stored in 70% ethanol at 4 °C until needed for imaging. Just prior to imaging, samples were further dehydrated in 100% ethanol, followed by critical point drying and gold sputter coating. For each sample, three separate locations were imaged using a Philips XL30 TMP scanning electron microscope, and collagen matrix fibril density and diameter were quantified using ImageJ (National Institute of Health, Bethesda, MD) as previously described [6].

2.10. Finite element model

Autodesk Inventor (Autodesk, San Rafael, CA) was used to generate representative 3D CAD renderings of both TMJ shape-specific, biconcave constructs as well as flat constructs. The respective geometries were then imported into ABAQUS/CAE (Dassault Systèmes, Vélizy-Villacoublay, France) to conduct the finite element analysis (FEA). A representative construct was modeled using a 4-noded linear tetrahedral mesh, or C3D4, with 52,636 elements, using a linear-elastic model. The goal of this analysis was to gain an understanding of the stress and strain distribution of the construct once it had fully relaxed under an elastic response. The material was defined based on the E_r acquired once the neotissue had fully relaxed during compressive testing at $t = 5$ wk, and a Poisson's ratio of 0.2 based on previous literature using a similar experimental model [39]. The nodes at the bottom of both models were constrained in the Z-direction to mimic the axial constraint of the agarose well in the experimental model; the
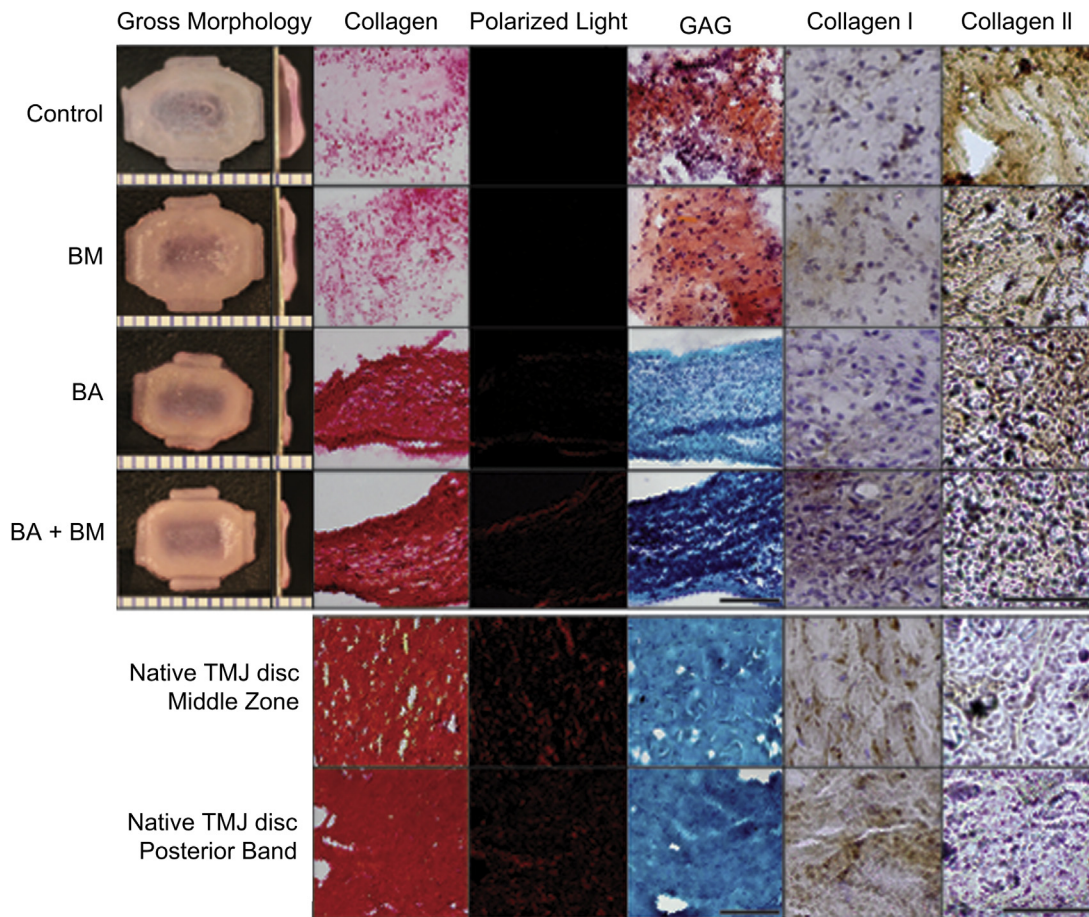

| | Gross Morphology | Collagen | Polarized Light | GAG | Collagen I | Collagen II |

Fig. 3. Gross morphology, histology and IHC of constructs at $t = 5$ wk (top) and native TMJ disc tissue (bottom). Shape-specific TMJ disc neotissue was treated with BM (passive axial compression), BA (C-ABC + TGF-β1), BM + BA, or left untreated (control). Engineered constructs were imaged with the middle zone on the left side of all images, transitioning into the band region toward the right, while entire middle zone and band region images were taken for native discal tissue. Collagen was stained using Picrosirious red and observed under polarized light to detect fibril organization and alignment. GAG was stained using Safranin O/Fast Green, while IHC was used to stain for collagen types I and II. BA and BM + BA treatments resulted in denser and more uniform collagen staining showing matrix alignment under polarized light, with enhanced organization observed in the combination-treated constructs. Like native TMJ disc tissue, BA and BM + BA neotissue stained negative for GAG. Finally, IHC found engineered neotissue to stain more strongly for collagen type II than type I, opposite of results for native tissue. Scale bar is 100 μm for histology, 150 μm for IHC, and the markings on the morphology images are 1 mm apart.

A Col/WW (%)

B Young's Modulus (MPa)

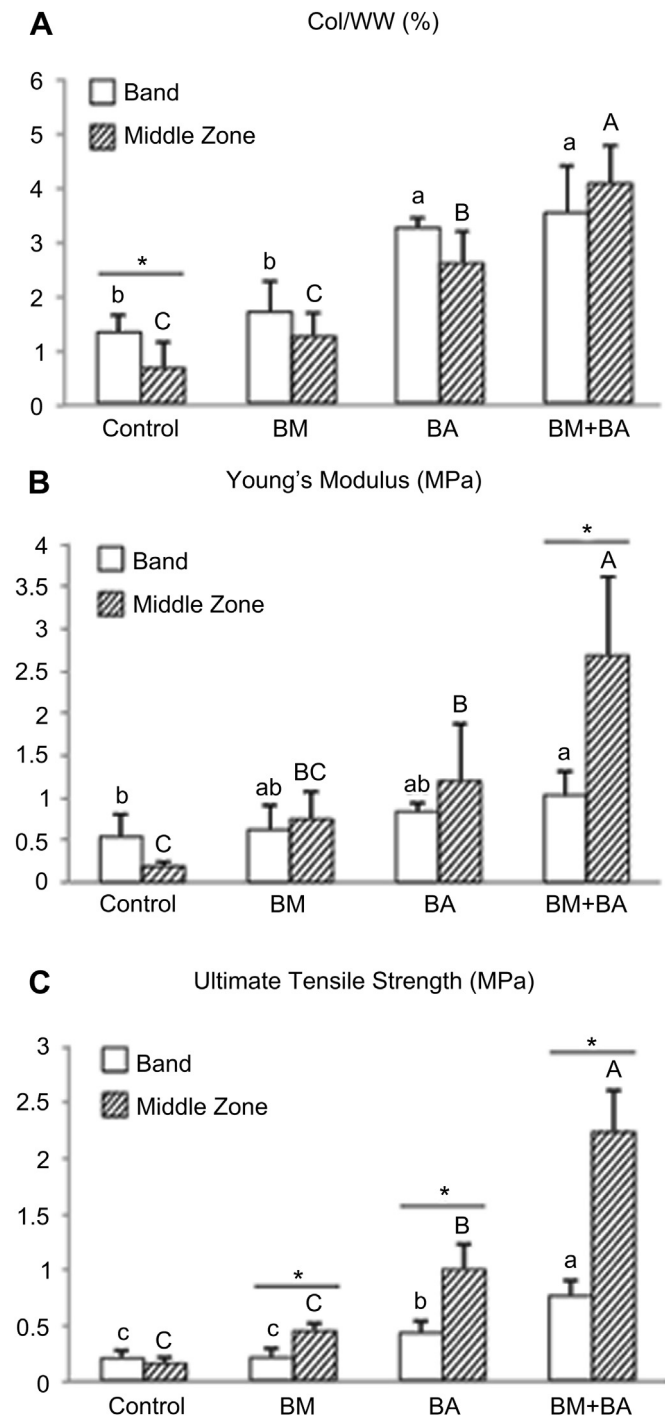**C** Ultimate Tensile Strength (MPa)

Fig. 4. Col/WW (A), Young's modulus (B), and ultimate tensile strength (C) of engineered neotissue at $t = 5$ wk. Shape-specific TMJ disc neotissue was treated with BM (passive axial compression), BA (C-ABC + TGF-β1), BM + BA, or left untreated (control). BM + BA promoted synergistic increases in terms of all three parameters (A–C) within the neotissue's middle zone over values achieved in the middle zone of controls. Bars not connected by the same letter are significantly different ($p < 0.05$).

same nodes were left unconstrained in the X- and Y-directions to capture the ability of the tissue to expand and contract within the well in these directions. The passive axial load was modeled as a pressure distribution across an area of 54 mm^2 on the top surface of the model. Parametric analysis was used to determine changes in the behavior of the models under passive axial load in response to altering either the E_r (from 10 to 100 kPa) or the load (from 1 g to 50 g), while keeping the other constant. For each case, a heat map of the resulting displacement, stress, and strain was obtained.

2.11. Statistics

To test the hypothesis that construct shape drives the anisotropic properties of the engineered tissue, a 2-tailed, paired Student's t-test was used to compare between construct regions for each exogenous stimulus. Separately, to test the hypothesis that the BM and BA stimuli were both significant factors toward increasing construct functional properties within a given region, a one-way analysis of variance (ANOVA; $n = 6$ per group) was used to analyze the data. When the one-way ANOVA showed significance ($p < 0.05$), a Tukey's HST *post hoc* test was applied.

Synergism was defined to occur if the combination treatment caused 1) a positive interaction on an additive scale and 2) results that were greater than those achieved by the addition of the results of the two singular treatments. Data for this study are represented as mean ± standard deviation (SD), with bars or groups marked by different letters signifying significant differences.

3. Results

3.1. Gross morphology, histology, and IHC

At $t = 5$ wk, all engineered tissue maintained the TMJ shape-specific biconcave shape. Control and BM constructs were significantly larger in all dimensions than both BA and BM + BA constructs (Table 1). While all constructs stained positive for collagen (Fig. 3), staining was denser and more uniform in BA and BM + BA constructs, reminiscent of native discal tissue. Polarized light showed no matrix alignment in control or BM constructs. Both BA and BM + BA constructs, however, exhibited birefringence under polarized light, with the BM + BA treatment promoting organization most similar to that of native tissue. Only control and BM constructs stained positive for GAG; BA, BM + BA and native TMJ disc stained negative for GAG. Finally, all neotissues stained stronger for collagen type II than type I, unlike native TMJ disc tissue, which had comparatively greater collagen type I staining.

3.2. Quantitative biochemistry

At the end of the 5-wk self-assembly period, the greatest collagen per wet weight (Col/WW) was measured in the middle zone of BM + BA constructs. Overall, BM + BA constructs exhibited a 162% and a synergistic 482% increase in Col/WW in the band region and middle zone, respectively, over control values for the same regions (Fig. 4A). The native TMJ disc Col/WW was measured to be 21.47 ± 6.13% and 18.71 ± 1.25% in the posterior band and middle zones, respectively. GAG per wet weight (GAG/WW) was significantly greater in the band of BM constructs compared to the band of control constructs, although no difference in GAG content was measured between the middle zones of these groups. GAG/WW values were 2.87 ± 1.36% and 5.41 ± 0.52% for the band region and 2.82 ± 0.76% and 2.88 ± 0.68% for the middle region of control and BM constructs, respectively. Similar to the native TMJ disc tissue, neither BA nor BM + BA constructs contained measurable sulfated GAG.

3.3. Stress-relaxation compressive testing

Stress-relaxation unconfined compression testing yielded similar trends in compressive properties at both 10% and 20% strain; therefore, results are provided only at 20%. Overall, control and BM constructs had significantly greater E_r than BA or BM + BA constructs. The E_r values of the band regions of control and BM constructs were significantly greater than those of their respective middle zones; this zonal difference was not seen for either BA or BM + BA constructs. The E_r values were 79.80 ± 23.56, 85.62 ± 17.49, 17.96 ± 3.94, and 21.39 ± 3.38 kPa for the band region and 24.57 ± 2.60, 34.92 ± 4.56, 18.78 ± 1.04, and 22.22 ± 2.79 kPa for the middle zone of control, BM, BA, and

BM + BA constructs, respectively. No significant difference in the E_r was found between the band region and middle zone of native TMJ disc tissue, having values of 19.92 ± 5.26 and 17.43 ± 2.43 kPa, respectively. Similar trends were found for E_i values at 20% strain, although the band regions of all treatments had significantly greater E_i values than their respective middle zones. The E_i values were 253.44 ± 46.50, 231.35 ± 61.34, 77.17 ± 9.32, and 71.62 ± 14.78 kPa for the band region and 71.62 ± 12.28, 86.12 ± 15.29, 39.60 ± 11.75, and 55.81 ± 14.85 kPa for the middle zone of control, BM, BA, and BM + BA constructs, respectively. For native TMJ disc tissue, E_i values of the band trended lower than that of the middle zone, at 95.14 ± 20.37 and 305.72 ± 134.41 kPa, respectively.

3.4. Uniaxial tensile testing

In the middle zone, uniaxial tensile testing found the BM + BA treatment to cause a synergistic 1368% increase in the E_Y over that of controls. Within BM + BA constructs, the middle zone had a significantly greater E_Y, at 2.6-fold of the band region. The BA treatment also significantly increased the E_Y of the middle zone over controls by 555% (Fig. 4B). The E_Y of the native TMJ disc trended higher in the middle zone when compared to the band, with values of 56.08 ± 21.76 and 33.79 ± 11.07 MPa, respectively. The BM + BA treatment resulted in a synergistic 1284% increase in the UTS of the middle zone over that of controls. The middle zone of BA constructs enhanced the UTS by 522% of controls. The middle zone of BM, BA, and BM + BA constructs all presented with a significantly greater UTS than their respective band regions, measuring 2.8-fold that of the band region in BM + BA constructs (Fig. 4C). The UTS of the middle zone of native TMJ disc tissue was found to trend higher than that of the band, with values of 29.98 ± 10.02 and 15.49 ± 2.13 MPa, respectively.

3.5. SEM

SEM images were quantified for both fibril density and diameter (Fig. 5). In controls, the middle zone had a highly disorganized and diffuse collagen matrix, while the band had much more densely packed fibrils. While the BM stimulus significantly increased the fibril diameter of the band region, the BA stimulus resulted in significant 48% and 39% increases in fibril diameter in the middle zone and band region, respectively, over those of controls. The BM + BA treatment significantly increased the fibril density of the middle zone over that of controls by 44.5%. The BM + BA treatment synergistically increased fibril diameters compared to all other groups, for example causing 85.8% and 64.6% increases in fibril diameter in the middle zone and band region, respectively, over control regions. Further, collagen bundles aligning predominantly in the AP direction were seen in the middle zones of both BA and BM + BA constructs.

3.6. FEA

Distinct differences in the displacement, stress, and strain distributions were found between the biconcave and flat models. A parametric analysis of load and compressive modulus showed that shape affected only the magnitude of the displacement, stress, and strain values but not their distribution. Specifically, the results scaled linearly with E_r and load. Fig. 6 shows displacement and strain results of a representative scenario: E_r of 25 kPa, Poisson's ratio of 0.2, and a load of 1 g. This set of parameters was found to result in 0.5%, 0.7%, and −0.9% strains in the *XX*, *YY*, and *ZZ* directions, respectively, within the middle zone of the biconcave model. In the flat model, the same parameters resulted in 0.1%, 0.1%, and −0.7% strains in the *XX*, *YY*, and *ZZ* directions. The biconcave shape thus increased these strains by approximately 5.4-times, 8.7-times, and 1.3-times values found in the flat model in each respective direction.
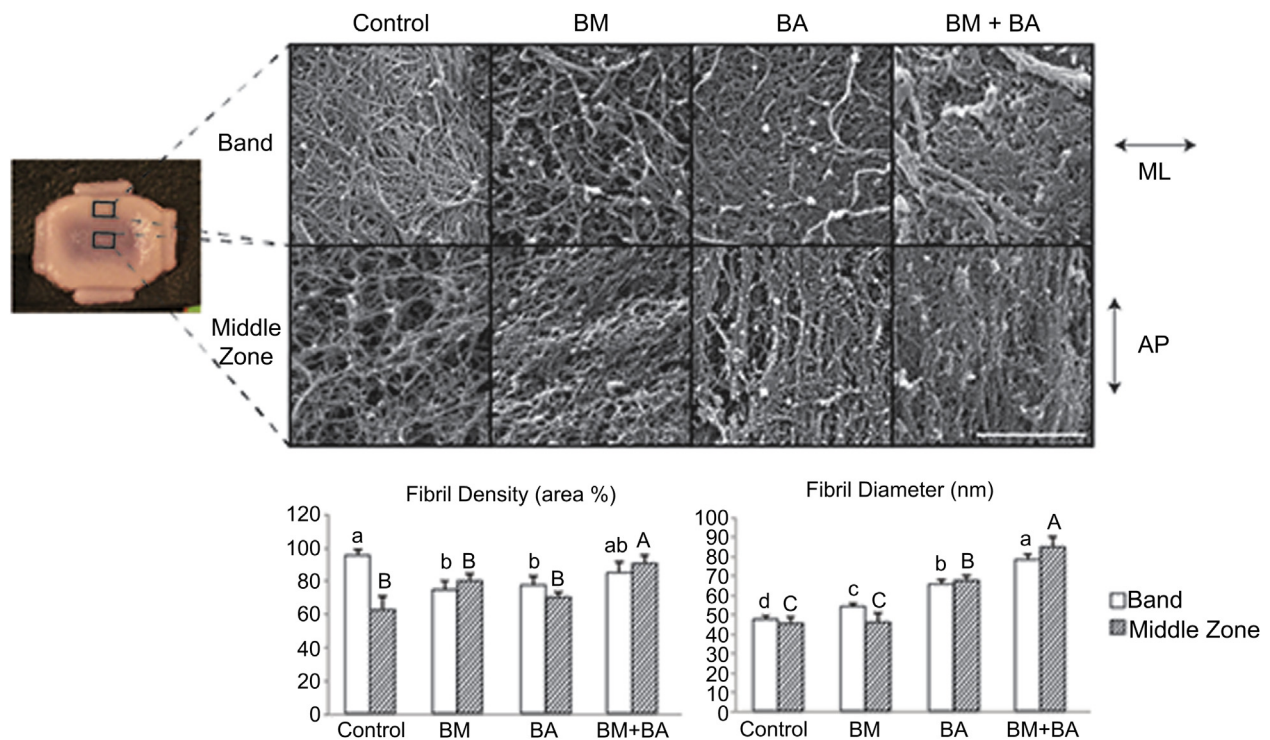

Fig. 5. SEM analysis of TMJ shape-specific neotissue at $t = 5$ wk, with images of control, BM, BA, and BM + BA for both band and middle zone regions. To measure collagen fibril diameter and density, three locations on three fibrocartilage constructs from each treatment were quantified. Results found BM + BA to promote synergistically thicker and significantly denser collagen fibrils in both construct regions overall treatments. Both BA and BM + BA constructs presented with bundling of fibers aligning predominantly in the AP direction of their respective middle zones. Bars not connected by the same letter are significantly different ($p < 0.05$). Scale bar is 2 μm. ML = mediolateral, AP = anteroposterior.
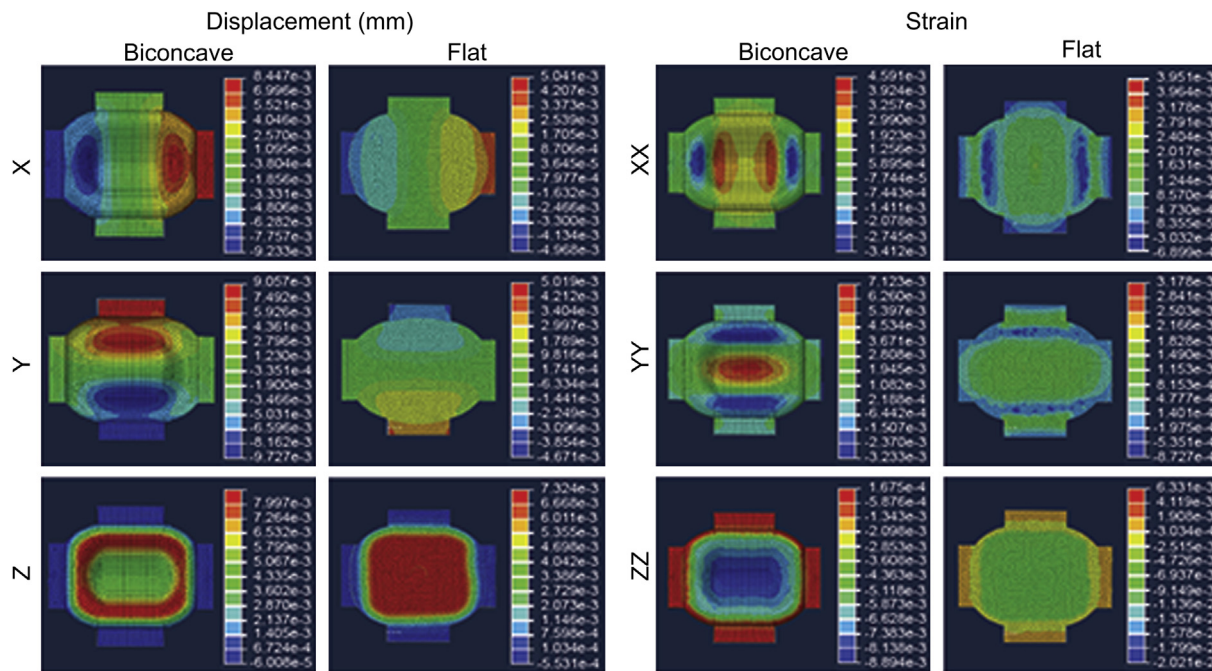
Fig. 6. Displacement and strain distributions of representative 3D CAD renderings using a 4-noded linear tetrahedral mesh of 52,636 elements of both biconcave and flat TMJ shape-specific constructs having $E_r = 25$ kPa, Poisson's ratio $= 0.2$, and a load of 1 g. Nodes at the bottom of both models were constrained in the Z-direction, and the passive axial load was modeled as a pressure distribution across an area of 54 mm^2 on the top surface of the models. This set of parameters resulted in 0.5%, 0.7%, and -0.9% strains in the XX, YY, and ZZ directions, respectively, within the middle zone of the biconcave model, and 0.1%, 0.1%, and -0.7% strains in the XX, YY, and ZZ directions, respectively, across the top surface of the flat model.

3.7. Comparison to the anisotropy of native tissue

An anisotropic functionality index (AFI) was developed to quantify the similarity between neofibrocartilage and native tissue. Ratios between the middle zone and band region of both engineered and native tissue were calculated for seven anisotropic factors. To determine how closely the engineered constructs maintained the aspect ratios of the shape-specific molds, two geometric anisotropic factors were calculated: ML:AP and B:MZ. To determine how the different exogenous stimuli affected the development of anisotropic functional properties, B:MZ ratios were calculated for five functional anisotropic factors: Col/WW (Col), E_r, E_i, E_Y, and UTS (Table 2). The AFI was calculated by taking the absolute value of the difference between native and engineered anisotropic factors, which were all equally weighed (Eq. (1)). The subscripts 'nt' and 'sf' represent values for native tissue and shape-specific fibrocartilage, respectively.

functional properties in the band compared to the middle zone, opposite those of native tissue. All other exogenous stimuli-treated constructs exhibited greater functional properties in the middle zone compared to the band region, representing native tissue trends.

4. Discussion

This study sought to determine the potential for engineering shape-specific, functionally anisotropic neofibrocartilage. Using self-assembled TMJ discs as a model system, results confirmed the hypothesis that combining biomechanical and biochemical cues in a shape-specific environment would drive *in vitro* fibrocartilage morphogenesis toward tissue-specific geometric shape and anisotropic functional properties. Specifically, the BM + BA treatment was found to synergistically increase Col/WW, Young's modulus, and ultimate tensile strength over controls by 482%, 1368%, and

$$\mathrm{AFI} = \frac{1}{7}\left(\left[1 - \left|\frac{(\mathrm{ML:AP_{nt}} - \mathrm{ML:AP_{sf}})}{\mathrm{ML:AP_{nt}}}\right|\right] + \left[1 - \left|\frac{(\mathrm{B:MZ_{nt}} - \mathrm{B:MZ_{sf}})}{\mathrm{B:MZ_{nt}}}\right|\right] + \left[1 - \left|\frac{(\mathrm{Col_{nt}} - \mathrm{Col_{sf}})}{\mathrm{Col_{nt}}}\right|\right] + \left[1 - \left|\frac{(E^r_{nt} - E^r_{sf})}{E^r_{nt}}\right|\right] \right.$$
$$\left. + \left[1 - \left|\frac{(E^i_{nt} - E^i_{sf})}{E^i_{nt}}\right|\right] + \left[1 - \left|\frac{(E^Y_{nt} - E^Y_{sf})}{E^Y_{nt}}\right|\right] + \left[1 - \left|\frac{(\mathrm{UTS_{nt}} - \mathrm{UTS_{sf}})}{\mathrm{UTS_{nt}}}\right|\right]\right) \qquad (1)$$

The AFI has a range of -1 to 1, with the sign of the value indicating whether, in general, anisotropic features are seen in the same direction as native tissue, which has an AFI of 1. AFI values for the engineered neotissue were -0.5, 0.5, 0.8, and 0.9 for control, BM, BA, and BM + BA constructs, respectively (Table 2). The negative value for the control indicates that this group had greater

1284%, respectively. The combination treatment was also found to promote synergistically thicker and significantly denser collagen fibrils aligning predominantly in the anteroposterior direction of the neotissue's middle zone, akin to that of native tissue. FEA confirmed strain distribution from the passive axial load within a shape-specific model to correspond to the anteroposterior

Table 2
Geometric and functional anisotropic factors used to calculate the anisotropic functionality index (AFI) for engineered shape-specific neotissue and native TMJ disc tissue, showing BM + BA-treated constructs to be closest to native discal tissue in terms of anisotropy. ML = mediolateral, AP = anteroposterior, B = band, MZ = middle zone.

Anisotropy factor	Control	BM	BA	BM + BA	Native TMJ disc
Geometry (ML:AP)	1.4	1.3	1.4	1.4	1.5
Geometry (B:MZ)	2.4	2.3	2.9	2.5	2.5
Col/WW (B:MZ)	1.4	1.5	0.9	1.2	1.1
E_r (B:MZ)	3.2	2.5	0.9	1.0	1.1
E_i (B:MZ)	3.5	2.7	1.9	1.2	1.3
E_Y (B:MZ)	3.3	0.9	0.7	0.4	0.6
UTS (B:MZ)	1.1	0.5	0.5	0.4	0.4
AFI	**−0.5**	**0.5**	**0.8**	**0.9**	**1.0**

alignment observed via SEM, suggesting that the biconcave shape plays an essential role in driving *in vitro* anisotropic neotissue development. Overall, with BM + BA resulting in an AFI of 0.9, results suggest the combination treatment promotes the development of functional anisotropy in shape-specific neotissues closest to that of native tissue. Thus, this study shows that a shape-specific environment with both biomechanical and bioactive cues is a powerful system to drive the internal and external architecture of scaffold-free *in vitro* tissues toward those of native tissue.

The system established in this study to drive *in vitro* tissue development is representative of native TMJ disc morphogenesis, which has been well characterized in the literature. Specifically, the articulating osseous structures of the joint precede development of the fibrocartilaginous disc, with the condyle and temporal bone forming during the 7th–10th wk of embryogenesis, followed by formation of the disc during wk 10–12 [40]. By wk 25 of development, the primordial disc turns into a dense fibrocartilaginous tissue [41]. The specific roles of the spatial constraints and forces exerted by the articulating surfaces as well as which molecular cues drive the disc's unique shape and anisotropic ECM organization during development remain unknown. Past work has found the critical period of TMJ morphogenesis to coincide with the onset of buccal, or mouth, cavity motion during embryogenesis [42]. Others have identified the link between molecular signaling and mechanical stimulation to be fundamental to the development of the fetal mandible and overall craniofacial growth [43]. This suggests that a similar interplay between stimuli is likewise essential for development of the TMJ. Thus, the shape-specific mold employed in this study recreates the spatial geometric boundaries set by the articulating surfaces prior to *in vivo* disc formation. Further, use of the BM + BA stimuli recapitulates the integral relationship between both biomechanical and biochemical cues during native discal development. Together, this combination of spatial, biomechanical, and biochemical cues may recreate the physiological interplay driving *in vivo* morphogenesis, improving overall *in vitro* tissue formation.

The ability for fibrocartilage to adapt to physical loads via mechanotransductive mechanisms is imperative for proper function; several studies have found the cells comprising such tissues to respond to mechanical loading *in vitro* [44–47]. Accordingly, this study introduced biconcave neofibrocartilage to passive axial loading from $t = 10–14$ d to increase the intrinsic mechanical forces imparted by the shape-specific molds, further driving the development of an anisotropic ECM. Results found the constructs to have tensile properties trending higher than those of controls. Further, addition of the BM stimulus enhanced the functional properties of the middle zone over those of the band region, reversing the AFI from −0.5 in controls to 0.5 in BM constructs (Table 2), closer to that of native tissue. Past work has

shown that loading of fibrocartilage initially increases the tissue's hydrostatic pressure, resulting in compaction of the matrix, cellular deformation, increased osmotic pressure, and physico-chemical changes that may lead to mechanotransduction [48–50]. Thus, it is conceivable that the BM stimulus likewise resulted in the changes necessary to result in a mechanotransductive response by the cells within the neotissue.

To understand the role of BM stimulation and construct shape in driving neotissue development, FEA was conducted to determine whether loading biconcave neotissue would 1) result in anisotropic strain distributions, and 2) result in sufficient magnitudes of strain to elicit mechanotransductive responses. FEA found the biconcave shape to result in anisotropic deformations having magnitudes known to result in mechanotransduction, with the highest stresses and strains localizing within the middle zone of the biconcave model (Fig. 6). Specifically, tensile strains in the *YY* direction were 1.6 times greater than those developing in the *XX* direction, and compressive strains in the *ZZ* direction were localized to the middle zone of the disc. This is physiologically significant, as this correlates with the greatest collagen alignment seen in the middle zone of the native TMJ disc tissue. Similar to the native tissue, FEA results correlated localized strains in the biconcave model to the same region where enhanced functional anisotropy was found in the engineered neotissue. Results therefore suggest that the biconcave shape uniquely conferred anisotropy, unlike flat constructs, which were also modeled. Thus, FEA results highlight the critical role of both shape and biomechanical cues toward *in vitro* development of anisotropic neotissues.

Low strain levels applied statically via BM stimulation over 5 d were found to enhance the anisotropic functional properties of the neotissue. Parametric analysis was conducted to determine how varying the E_r from 10 kPa to 100 kPa affected the resulting strain magnitudes. Based on prior work on self-assembled tissues, an E_r of 10 kPa was estimated to correspond to construct stiffness at $t = 10$ d [25], while an E_r of 25 kPa was determined from stiffness measurement of constructs at $t = 5$ wk. Thus, during the time of initial loading ($t = 10$ d), the 1 g load used in this experiment resulted in strains of 1.1%, 1.8% and −2.2% in the *XX*, *YY*, and *ZZ* directions, respectively. Using an E_r of 25 kPa reduces the strains to approximately 0.5%, 0.7%, and −0.9% in the *XX*, *YY*, and *ZZ* directions, respectively. These results may seem counterintuitive, as past work has typically associated static loading with a dose-dependent decrease in synthetic ability; such studies, however, have focused on the effects of static strains of 10% or greater [51,52]. A more recent study subjecting engineered articular cartilage to 2–4% static biaxial strains during $t = 14–28$ d of culture found these low strain levels to increase the collagen content of the tissue by 17% [53]. The present study's results indicate that the threshold of load application required to elicit a cellular response is quite low. This may be relevant in other applications employing relatively stiff biomaterials, which may stress-shield cells seeded within them. In such biomaterials, loading levels can be tailored to take into account stress-shielding, thus ensuring a low strain level capable of promoting anabolic cellular responses. Overall, it is likely that strains resulting from the 1 g load were low enough to promote an anabolic, mechanotransductive response by the cells in the biconcave neotissue, meriting future work to understand the possible mechanotransductive benefits of low static strain on engineered neotissue development.

The BA treatment consisting of C-ABC and TGF-β1 was found to promote a more functionally mature, organized collagen matrix within the TMJ shape-specific neotissue. Specifically, BA-treated neotissue had an AFI of 0.8, which was closer to the AFI of native tissue compared to that of either control or BM constructs (Table 2).

Whereas the BM stimulus only caused the neotissue's functional properties to trend higher, the BA stimulus significantly enhanced the functional properties of the tissue. This is likely due to the significant contraction of the tissue following C-ABC application. Specifically, the outer diameter of the major axis of the constructs were decreased by 20% in BA-treated constructs compared to controls, while the band and middle zone of these constructs were decreased 46% and 60% in thickness, respectively. Such large changes in dimension during treatment with C-ABC likely resulted in substantial strains in the BA-treated neotissue, thereby prompting the cells to remodel the matrix in the direction of maximum strain. With past work showing the sensitivity of fibro-cartilage cells to strains [54], this provides a possible rationale for why the BA stimulus promoted matrix organization in an aniso-tropic manner and significantly enhanced neotissue properties compared to the 1 g axial compressive load.

To capture the critical interplay between biomechanical and biochemical cues for native fibrocartilage development, the present study treated shape-specific neotissue with both BM and BA stimuli. The BM + BA stimulus was found to synergistically enhance the Col/WW, collagen fibril diameters, and tensile properties over controls. Natively, collagen fibrils of the rat TMJ disc have been measured to range from 30 to 60 nm in diameter from birth to $t = 2$ wk. By $t = 1$ yr, fibril diameters ranged from 10 to 140 nm, overall density significantly increased, and the bundling of fibrils into fibers become obvious throughout the tissue [55]. This broadening of the distribution of fibril diameters and the presence of bundles of collagen, which is typical during the development of highly collagenous tissues, have been directly correlated to increased tensile properties [56,57]. In the present study, control tissue had collagen fibril diameters of 45 ± 3 nm at $t = 5$ wk, which were synergistically increased to 85 ± 5 nm following treatment with BM + BA, concomitant with bundling of collagen fibrils, and a significant increase in density. Thus, results suggest that the BM + BA treatment promotes *in vitro* maturation of the tissue reminiscent of the maturation observed during native tissue development. Further, both SEM and polarized light microscopy confirmed anteroposterior alignment of the collagen fibrils in BM + BA construct middle zones, reminiscent of native tissue fiber orientation. Together, the BM and BA treatments promoted shape-specific constructs to have an AFI closer to that of native discal tissue compared to either stimulus alone or controls, highlighting the essential role of this combination of stimuli toward anisotropic neotissue development.

5. Conclusions

In this study, methods were developed to 1) engineer the first self-assembled, shape-specific TMJ discs and 2) promote matrix anisotropy within neotissues. This approach, employing spatial, biomechanical, and biochemical cues, offers much promise toward the development of a simple, yet effective, platform technology for engineering clinically relevant fibrocartilaginous tissues. Further, with past work finding neocartilage capable of post-implantation maturation [6], it is expected that anisotropic engineered fibro-cartilaginous discs will be prompted to further mature and adapt their ECM according to the native *in vivo* joint environment upon implantation. Fundamentally, this study offers insight on the ability to achieve physiologic anisotropy of biomaterials through the strategic application of stimuli. Efforts to better understand the biomechanical and biochemical cues present during native joint morphogenesis, as well as the mechanisms behind fibrocartilage mechanotransduction, will greatly aid tissue engineering efforts toward developing clinically relevant tissues.

References

[1] Huey DJ, Hu JC, Athanasiou KA. Unlike bone, cartilage regeneration remains elusive. Science 2012;338:917–21.
[2] Ben-Yishay A, Grande DA, Schwartz RE, Menche D, Pitman MD. Repair of articular cartilage defects with collagen-chondrocyte allografts. Tissue Eng 1995;1:119–33.
[3] Lee CH, Cook JL, Mendelson A, Moioli EK, Yao H, Mao JJ. Regeneration of the articular surface of the rabbit synovial joint by cell homing: a proof of concept study. Lancet 2010;376:440–8.
[4] Makris EA, Hu JC, Athanasiou KA. Hypoxia-induced collagen crosslinking as a mechanism for enhancing mechanical properties of engineered articular cartilage. Osteoarthr Cartil 2013;21:634–41.
[5] Makris EA, Macbarb RF, Responte DJ, Hu JC, Athanasiou KA. A copper sulfate and hydroxylysine treatment regimen for enhancing collagen cross-linking and biomechanical properties in engineered neocartilage. FASEB J 2013;6: 2421–30.
[6] Responte DJ, Arzi B, Natoli RM, Hu JC, Athanasiou KA. Mechanisms underlying the synergistic enhancement of self-assembled neocartilage treated with chondroitinase-ABC and TGF-beta1. Biomaterials 2012;33:3187–94.
[7] Woodfield TB, Guggenheim M, von Rechenberg B, Riesle J, van Blitterswijk CA, Wedler V. Rapid prototyping of anatomically shaped, tissue-engineered im-plants for restoring congruent articulating surfaces in small joints. Cell Prolif 2009;42:485–97.
[8] Xie J, Han Z, Naito M, Maeyama A, Kim SH, Kim YH, et al. Articular cartilage tissue engineering based on a mechano-active scaffold made of poly(L-lactide-co-epsilon-caprolactone): in vivo performance in adult rabbits. J Biomed Mater Res B Appl Biomater 2010;94:80–8.
[9] Ballyns JJ, Gleghorn JP, Niebrzydowski V, Rawlinson JJ, Potter HG, Maher SA, et al. Image-guided tissue engineering of anatomically shaped implants via MRI and micro-CT using injection molding. Tissue Eng Part A 2008;14: 1195–202.
[10] Blanquer SB, Sharifi S, Grijpma DW. Development of poly(trimethylene car-bonate) network implants for annulus fibrosus tissue engineering. J Appl Biomater Funct Mater 2013;10:177–84.
[11] Brown BN, Chung WL, Almarza AJ, Pavlick MD, Reppas SN, Ochs MW, et al. Inductive, scaffold-based, regenerative medicine approach to reconstruc-tion of the temporomandibular joint disk. J Oral Maxillofac Surg 2012;70: 2656–68.
[12] Brown BN, Chung WL, Pavlick M, Reppas S, Ochs MW, Russell AJ, et al. Extracellular matrix as an inductive template for temporomandibular joint meniscus reconstruction: a pilot study. J Oral Maxillofac Surg 2011;69: e488–505.
[13] Kang SW, Son SM, Lee JS, Lee ES, Lee KY, Park SG, et al. Regeneration of whole meniscus using meniscal cells and polymer scaffolds in a rabbit total menis-cectomy model. J Biomed Mater Res A 2006;78:659–71.
[14] Mandal BB, Park SH, Gil ES, Kaplan DL. Multilayered silk scaffolds for meniscus tissue engineering. Biomaterials 2011;32:639–51.
[15] Pan Y, Chu T, Dong S, Hao Y, Ren X, Wang J, et al. Cells scaffold complex for intervertebral disc anulus fibrosus tissue engineering: in vitro culture and product analysis. Mol Biol Rep 2012;39:8581–94.
[16] Baker BM, Mauck RL. The effect of nanofiber alignment on the maturation of engineered meniscus constructs. Biomaterials 2007;28:1967–77.
[17] Courtney T, Sacks MS, Stankus J, Guan J, Wagner WR. Design and analysis of tissue engineering scaffolds that mimic soft tissue mechanical anisotropy. Biomaterials 2006;27:3631–8.
[18] Lee CH, Shin HJ, Cho IH, Kang YM, Kim IA, Park KD, et al. Nanofiber alignment and direction of mechanical strain affect the ECM production of human ACL fibroblast. Biomaterials 2005;26:1261–70.
[19] Hoben GM, Hu JC, James RA, Athanasiou KA. Self-assembly of fibrochon-drocytes and chondrocytes for tissue engineering of the knee meniscus. Tissue Eng 2007;13:939–46.
[20] MacBarb RF, Makris EA, Hu JC, Athanasiou KA. A chondroitinase-ABC and TGF-beta1 treatment regimen for enhancing the mechanical properties of tissue-engineered fibrocartilage. Acta Biomater 2013;9:4626–34.
[21] Aufderheide AC, Athanasiou KA. Assessment of a bovine co-culture, scaffold-free method for growing meniscus-shaped constructs. Tissue Eng 2007;13: 2195–205.
[22] Kalpakci KN, Kim EJ, Athanasiou KA. Assessment of growth factor treatment on fibrochondrocyte and chondrocyte co-cultures for TMJ fibrocartilage en-gineering. Acta Biomater 2011;7:1710–8.
[23] Revell CM, Reynolds CE, Athanasiou KA. Effects of initial cell seeding in self assembly of articular cartilage. Ann Biomed Eng 2008;36:1441–8.
[24] Hu JC, Athanasiou KA. A self-assembling process in articular cartilage tissue engineering. Tissue Eng 2006;12:969–79.

[25] Ofek G, Revell CM, Hu JC, Allison DD, Grande-Allen KJ, Athanasiou KA. Matrix development in self-assembly of articular cartilage. PLoS One 2008;3:e2795.
[26] Meller R, Schiborra F, Brandes G, Knobloch K, Tschernig T, Hankemeier S, et al. Postnatal maturation of tendon, cruciate ligament, meniscus and articular cartilage: a histological study in sheep. Ann Anat 2009;191:575–85.
[27] Mikic B, Isenstein AL, Chhabra A. Mechanical modulation of cartilage structure and function during embryogenesis in the chick. Ann Biomed Eng 2004;32:18–25.
[28] Roddy KA, Prendergast PJ, Murphy P. Mechanical influences on morphogenesis of the knee joint revealed through morphological, molecular and computational analysis of immobilised embryos. PLoS One 2011;6:e17526.
[29] Natoli RM, Revell CM, Athanasiou KA. Chondroitinase ABC treatment results in greater tensile properties of self-assembled tissue-engineered articular cartilage. Tissue Eng Part A 2009;15:3119–28.
[30] Hu JC, Athanasiou KA. The effects of intermittent hydrostatic pressure on self-assembled articular cartilage constructs. Tissue Eng 2006;12:1337–44.
[31] Huey DJ, Athanasiou KA. Tension-compression loading with chemical stimulation results in additive increases to functional properties of anatomic meniscal constructs. PLoS One 2011;6:e27857.
[32] Elder BD, Athanasiou KA. Effects of confinement on the mechanical properties of self-assembled articular cartilage constructs in the direction orthogonal to the confinement surface. J Orthop Res 2008;26:238–46.
[33] Almarza AJ, Bean AC, Baggett LS, Athanasiou KA. Biochemical analysis of the porcine temporomandibular joint disc. Br J Oral Maxillofac Surg 2006;44:124–8.
[34] Detamore MS, Orfanos JG, Almarza AJ, French MM, Wong ME, Athanasiou KA. Quantitative analysis and comparative regional investigation of the extracellular matrix of the porcine temporomandibular joint disc. Matrix Biol 2005;24:45–57.
[35] Allen KD, Athanasiou KA. A surface-regional and freeze-thaw characterization of the porcine temporomandibular joint disc. Ann Biomed Eng 2005;33:951–62.
[36] Allen KD, Athanasiou KA. Viscoelastic characterization of the porcine temporomandibular joint disc under unconfined compression. J Biomech 2006;39:312–22.
[37] Almarza AJ, Athanasiou KA. Seeding techniques and scaffolding choice for tissue engineering of the temporomandibular joint disk. Tissue Eng 2004;10:1787–95.
[38] Natoli RM, Responte DJ, Lu BY, Athanasiou KA. Effects of multiple chondroitinase ABC applications on tissue engineered articular cartilage. J Orthop Res 2009;27:949–56.
[39] Gunja NJ, Huey DJ, James RA, Athanasiou KA. Effects of agarose mould compliance and surface roughness on self-assembled meniscus-shaped constructs. J Tissue Eng Regen Med 2009;3:521–30.
[40] Van der Linden EJ, Burdi AR, de Jongh HJ. Critical periods in the prenatal morphogenesis of the human lateral pterygoid muscle, the mandibular condyle, the articular disk, and medial articular capsule. Am J Orthod Dentofacial Orthop 1987;91:22–8.
[41] Radlanski RJ, Lieck S, Bontschev NE. Development of the human temporomandibular joint. Computer-aided 3D-reconstructions. Eur J Oral Sci 1999;107:25–34.
[42] Humphrey T. The development of mouth opening and related reflexes involving the oral area of human fetuses. Ala J Med Sci 1968;5:126–57.
[43] Radlanski RJ, Renz H. Genes, forces, and forms: mechanical aspects of prenatal craniofacial development. Dev Dyn 2006;235:1219–29.
[44] Deschner J, Rath-Deschner B, Agarwal S. Regulation of matrix metalloproteinase expression by dynamic tensile strain in rat fibrochondrocytes. Osteoarthr Cartil 2006;14:264–72.
[45] Ferretti M, Madhavan S, Deschner J, Rath-Deschner B, Wypasek E, Agarwal S. Dynamic biophysical strain modulates proinflammatory gene induction in meniscal fibrochondrocytes. Am J Physiol Cell Physiol 2006;290:C1610–5.
[46] Gilbert HT, Hoyland JA, Freemont AJ, Millward-Sadler SJ. The involvement of interleukin-1 and interleukin-4 in the response of human annulus fibrosus cells to cyclic tensile strain: an altered mechanotransduction pathway with degeneration. Arthritis Res Ther 2011;13:R8.
[47] Le Maitre CL, Frain J, Millward-Sadler J, Fotheringham AP, Freemont AJ, Hoyland JA. Altered integrin mechanotransduction in human nucleus pulposus cells derived from degenerated discs. Arthritis Rheum 2009;60:460–9.
[48] Armstrong CG, Lai WM, Mow VC. An analysis of the unconfined compression of articular cartilage. J Biomech Eng 1984;106:165–73.
[49] Gray ML, Pizzanelli AM, Grodzinsky AJ, Lee RC. Mechanical and physiochemical determinants of the chondrocyte biosynthetic response. J Orthop Res 1988;6:777–92.
[50] Ragan PM, Chin VI, Hung HH, Masuda K, Thonar EJ, Arner EC, et al. Chondrocyte extracellular matrix synthesis and turnover are influenced by static compression in a new alginate disk culture system. Arch Biochem Biophys 2000;383:256–64.
[51] Davisson T, Kunig S, Chen A, Sah R, Ratcliffe A. Static and dynamic compression modulate matrix metabolism in tissue engineered cartilage. J Orthop Res 2002;20:842–8.
[52] Imler SM, Doshi AN, Levenston ME. Combined effects of growth factors and static mechanical compression on meniscus explant biosynthesis. Osteoarthr Cartil 2004;12:736–44.
[53] Fan JC, Waldman SD. The effect of intermittent static biaxial tensile strains on tissue engineered cartilage. Ann Biomed Eng 2010;38:1672–82.
[54] Sanchez-Adams J, Athanasiou KA. Biomechanics of meniscus cells: regional variation and comparison to articular chondrocytes and ligament cells. Biomech Model Mechanobiol 2012;11:1047–56.
[55] Ahn HJ, Paik SK, Choi JK, Kim HJ, Ahn DK, Cho YS, et al. Age-related changes in the microarchitecture of collagen fibrils in the articular disc of the rat temporomandibular joint. Arch Histol Cytol 2007;70:175–81.
[56] Diamant J, Keller A, Baer E, Litt M, Arridge RG. Collagen; ultrastructure and its relation to mechanical properties as a function of ageing. Proc R Soc Lond B Biol Sci 1972;180:293–315.
[57] Parry DA. The molecular and fibrillar structure of collagen and its relationship to the mechanical properties of connective tissue. Biophys Chem 1988;29:195–209.